Using Idealized Coherent Structures to Parameterize Momentum Fluxes in a PBL Mass-Flux Model

CARA-LYN LAPPEN AND DAVID A. RANDALL

Department of Atmospheric Science, Colorado State University, Fort Collins, Colorado

(Manuscript received 3 September 2004, in final form 30 December 2004)

ABSTRACT

In 2001, the authors presented a higher-order mass-flux model called assumed distributions with higher-order closure (ADHOC), which represents the large eddies of the planetary boundary layer (PBL) in terms of an assumed joint distribution of the vertical velocity and scalars such as potential temperature or water vapor mixing ratio. ADHOC is intended for application as a PBL parameterization. It uses the equations of higher-order closure to predict selected moments of the assumed distribution, and diagnoses the parameters of the distribution from the predicted moments. Once the parameters of the distribution are known, all moments of interest can be computed.

The first version of ADHOC was incomplete in that the horizontal momentum equations, the vertical fluxes of horizontal momentum, the contributions to the turbulence kinetic energy from the horizontal wind, and the various pressure terms involving covariances between pressure and other variables were not incorporated into the assumed distribution framework. Instead, these were parameterized using standard methods.

This paper describes an updated version of ADHOC. The new version includes representations of the horizontal winds and momentum fluxes that are consistent with the mass-flux framework of the model. The assumed joint probability distribution is replaced by an assumed joint spatial distribution based on an idealized coherent structure, such as a plume or roll. The horizontal velocity can then be determined using the continuity equation, and the momentum fluxes and variances are computed directly by spatial integration. These expressions contain unknowns that involve the parameters of the assumed coherent structures. Methods are presented to determine these parameters, which include the radius of convective updrafts and downdrafts and the wavelength, tilt, and orientation angle of the convective rolls. The parameterization is tested by comparison with statistics computed from large-eddy simulations. In a companion paper, the results of this paper are built on to determine the perturbation pressure terms needed by the model.

1. Introduction

In 2001, we (Lappen and Randall 2001a,b,c; hereafter LRa,b,c) described a new type of mass-flux model called assumed distributions with higher-order closure (ADHOC). ADHOC is intended for use as a planetary boundary layer (PBL) parameterization in large-scale models. It represents the PBL's large eddies in terms of an assumed joint distribution of the vertical velocity and scalars such as potential temperature or water vapor mixing ratio. The joint distribution is based on the assumed existence of idealized coherent structures, such as plumes or rolls. ADHOC uses the equations of higher-order closure to predict selected moments of the assumed distribution, and diagnoses the parameters of the distribution from the predicted moments. Once the parameters have been determined, all moments of interest can be computed. To close the model, we used analogs between ADHOC's equations and those of higher-order closure models (see also de Roode et al. 2000). For example, ADHOC's dissipation closure is an adaptation of the one proposed by Bougeault and André (1986; see LRb for a discussion).

The 2001 version of ADHOC did not incorporate the horizontal velocity components into the assumed distribution framework; the vertical flux of horizontal momentum and all pressure covariances were included using conventional second-order closure methods. We chose this route because, quite frankly, we did not see

Corresponding author address: Dr. Cara-Lyn Lappen, Dept. of Atmospheric Science, Colorado State University, Fort Collins, CO 80523.
E-mail: lappen@atmos.colostate.edu

a satisfactory alternative at the time. The mass-flux approach has been used to parameterize momentum transports by deep cumulus convection (e.g., Wu and Yanai 1994), but with little in the way of supporting tests. To our knowledge, the only study that had investigated the use of standard mass-flux formulas to represent momentum fluxes in a PBL model is that of Brown (1999). In a study of shallow-cumulus clouds, he found that the representation of momentum fluxes with an assumed joint distribution was poor compared with using the same approach for scalar fluxes. He assumed that the horizontal and vertical velocities were perfectly correlated, with joint top-hat profiles.

The use of conventional closure methods for the momentum fluxes and the pressure covariances in ADHOC gave rise to some inconsistencies. It was a temporary compromise.

The current paper begins the description of ADHOC2, which includes consistent representations of the horizontal winds including the momentum fluxes. ADHOC2 is based on a phenomenological approach. We assume idealized geometries for the PBL's coherent structures, consistent with the mass-flux framework. This means that we move beyond assumed probability distributions and adopt assumed spatial distributions. In particular, we consider idealized versions of two commonly occurring coherent structures, namely unsheared plumes (cylindrical geometry with the cylinder's axis perpendicular to the ground) and sheared rolls (homogeneity in one horizontal direction). We use the assumed geometries to derive velocity fields. Covariances such as momentum fluxes are then constructed directly by spatial integration. The expressions that we obtain for these higher moments contain unknown parameters related to the geometry of the circulations. These include the radii of the updraft and downdraft for the unsheared plume case and the tilt, orientation angle, and cross-roll wavelength of the roll circulations. We provide a method for diagnosing these parameters using quantities that are available in ADHOC2. To our knowledge, this is the first time that a PBL parameterization has been used to diagnose such parameters.

In section 2, we discuss the case of axisymmetric convection with no mean flow. This is the plume version of ADHOC2. In section 3, we examine a slab-symmetric case with both buoyancy and shear (a roll). This is the roll version of ADHOC2. In section 4, we discuss the solution of the equations for the roll case. In section 5, we give a summary, discuss some limitations of our approach, and outline possible future directions, including speculations on how the plume and roll versions of ADHOC2 can be combined. Throughout the paper, our results are compared to data generated using the large-eddy simulation (LES) model described by Khairoutdinov and Randall (2003).

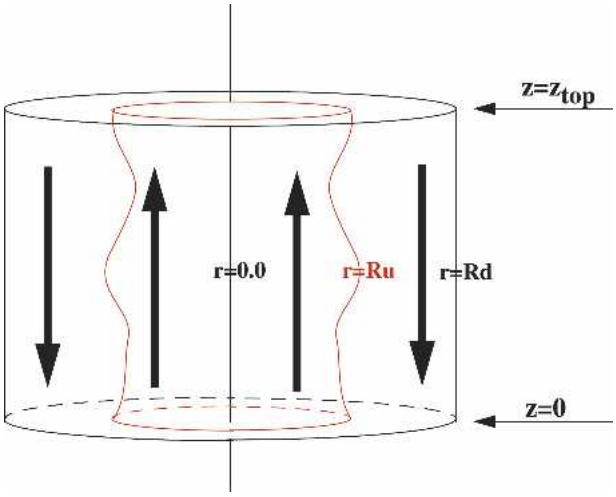

FIG. 1. Idealization of the clear convective geometry. The inner and outer cylinders are concentric circles: R_u (R_d) is the distance from the updraft center to the outer edge of the updraft (downdraft). Note that R_u varies with height.

2. Axisymmetric free convection

Consider an ensemble of axisymmetric convective plumes (Fig. 1) in the absence of a mean flow. Obviously in this case there is no vertical flux of horizontal momentum. Plumes in free convective PBLs have been extensively investigated using both observations (e.g., Willis and Deardorff 1974) and LES (e.g., Moeng 1984; Schumann and Moeng 1991).

To analyze the circulation associated with a plume, we adopt cylindrical coordinates, with radial coordinate r. In Fig. 1, the inner cylinder of radius $r = R_i(z)$ (the subscript stands for inner) represents a convective draft across which the vertical velocity is horizontally uniform, while the annulus between the inner and outer cylinders represents the compensating draft of the opposite sign.[1] The radius of the outer cylinder, that is, the total diameter of the plume, is denoted by R_o (the subscript stands for outer). In this paper we assume that R_o is independent of height and time and that the plumes are closely packed. Obviously they cannot really be closely packed if they are cylindrical, that is, with circular planforms. Hexagonal (or triangular or rectangular) symmetry would be required for true close packing, but we prefer to avoid the additional complexity of

[1] Here draft can refer to either an updraft or a downdraft.

solving the equations in those geometries. This issue can be revisited in the future.

The fractional area occupied by the inner cylinder is

$$\sigma_i(z) = \left[\frac{R_i(z)}{R_o}\right]^2. \tag{1}$$

We assume that the vertical velocity and thermodynamic variables are horizontally uniform within the inner cylinder and the surrounding annulus, but in general they can be discontinuous across $r = R_i(z)$. The radial velocity and pressure must vary radially, as discussed below. The regions denoted by the subscripts i and o in Eq. (1) represent the updraft, and the downdraft, (to use the terminology of LRa–c), but here we make no assumption about which region is which. In the plume version of ADHOC2, σ_i and w_i are predicted, using equations presented by LRa; the sign of the predicted w_i obviously reveals which region is the updraft and which is the downdraft. As shown by Randall et al. (1992),

$$\overline{w} = \sigma_i w_i + (1 - \sigma_i) w_o, \tag{2}$$

$$\begin{aligned}\overline{w'^2} &= \sigma_i(w_i - \overline{w})^2 + (1 - \sigma_i)(w_o - \overline{w})^2 \\ &= \sigma_i(1 - \sigma_i)(w_i - w_o)^2.\end{aligned} \tag{3}$$

In the remainder of this section, we use the vertical profiles of w_i and w_o, assumed known, along with the continuity equation to work out the radial dependence of the radial velocity component. We assume that there is no velocity component in the azimuthal direction. We also derive the boundary conditions that apply across $r = R_i(z)$.

We begin with the radial boundary conditions. Obviously, we must require that

$$v_r(0) = 0. \tag{4}$$

The mass flow rate must be continuous across $r = R_i$. This implies that

$$\left[\rho\left(\frac{\partial R_i}{\partial t} + w\frac{\partial R_i}{\partial z} - v_r\right)\right]_{R_i+\varepsilon} = \left[\rho\left(\frac{\partial R_i}{\partial t} + w\frac{\partial R_i}{\partial z} - v_r\right)\right]_{R_i-\varepsilon}, \tag{5}$$

where $(\,)_{R_i-\varepsilon}$ and $(\,)_{R_i+\varepsilon}$ denotes values evaluated just inside and just outside $r = R_i$, respectively (Randall and Huffman 1982). We also assume that no mass crosses $r = R_o$ so that

$$\left[\rho\left(\frac{\partial R_o}{\partial t} + w_o\frac{\partial R_o}{\partial z} - v_r\right)\right]_{R_o+\varepsilon} = 0. \tag{6}$$

Using our assumption that R_o is independent of height and time, we see from (6) that

$$v_r(R_o) = 0. \tag{7}$$

At this point, we adopt the Bousinesq form of the continuity equation; that is,

$$\frac{1}{r}\frac{\partial}{\partial r}(rv_r) + \frac{\partial w}{\partial z} = 0. \tag{8}$$

As discussed earlier, we assume that the vertical velocity is horizontally uniform across the inner cylinder, and horizontally uniform again, with a different value, across the outer annulus. This is analogous to the assumption used in mass-flux models (e.g., LRa; Betts 1976; Wang and Albrecht 1990). Integrating (8) from $r = 0$ to an arbitrary value of r inside the inner cylinder, and using (4), we find that the radial velocity satisfies

$$v_r(r) = -\left(\frac{r}{2}\right)\frac{\partial w_i}{\partial z} \quad \text{for} \quad r < R_i. \tag{9}$$

The Bousinesq approximation also allows us to simplify Eq. (5) to

$$\left(w\frac{\partial R_i}{\partial z} - v_r\right)_{R_i+\varepsilon} \cong \left(w\frac{\partial R_i}{\partial z} - v_r\right)_{R_i-\varepsilon}. \tag{10}$$

From (10), we see that

$$(v_r)_{R_i+\varepsilon} = (v_r)_{R_i-\varepsilon} + (w_o - w_i)\frac{\partial R_i}{\partial z}, \tag{11}$$

which tells us that v_r is discontinuous at $r = R_i$ when R_i varies with height. By combining (9) and (11), we obtain

$$(v_r)_{R_i+\varepsilon} = -\frac{R_i \partial w_i}{2\partial z} + \frac{\partial R_i}{\partial z}(w_o - w_i). \tag{12}$$

Similarly, integrating Eq. (8) from an arbitrary point in the outer cylinder to $r = R_o + \varepsilon$ and using (10), we obtain

$$rv_r(r) = \frac{\partial w_o}{\partial z}\left(\frac{R_o^2}{2} - \frac{r^2}{2}\right) \quad \text{for} \quad R_i < r \le R_o. \tag{13}$$

Applying (13) at $r = R_i + \varepsilon$ and using (12), we find that the area-averaged vertical velocity is equal to zero (see LRa). Because we use (9) outward from $r = 0$ and (13) inward from $r = R_o + \varepsilon$, we are ensured that (10) is satisfied. Suppose that $w_i(z)$, $w_o(z)$, $R_i(z)$, and R_o were known. Then, $v_r(r, z)$ could be evaluated as outlined above. The perturbation pressure field could then be determined, using methods to be described elsewhere (Lappen and Randall 2005, manuscript submitted to *J. Atmos. Sci.*). ADHOC predicts $\sigma_i(z)$. If we know either

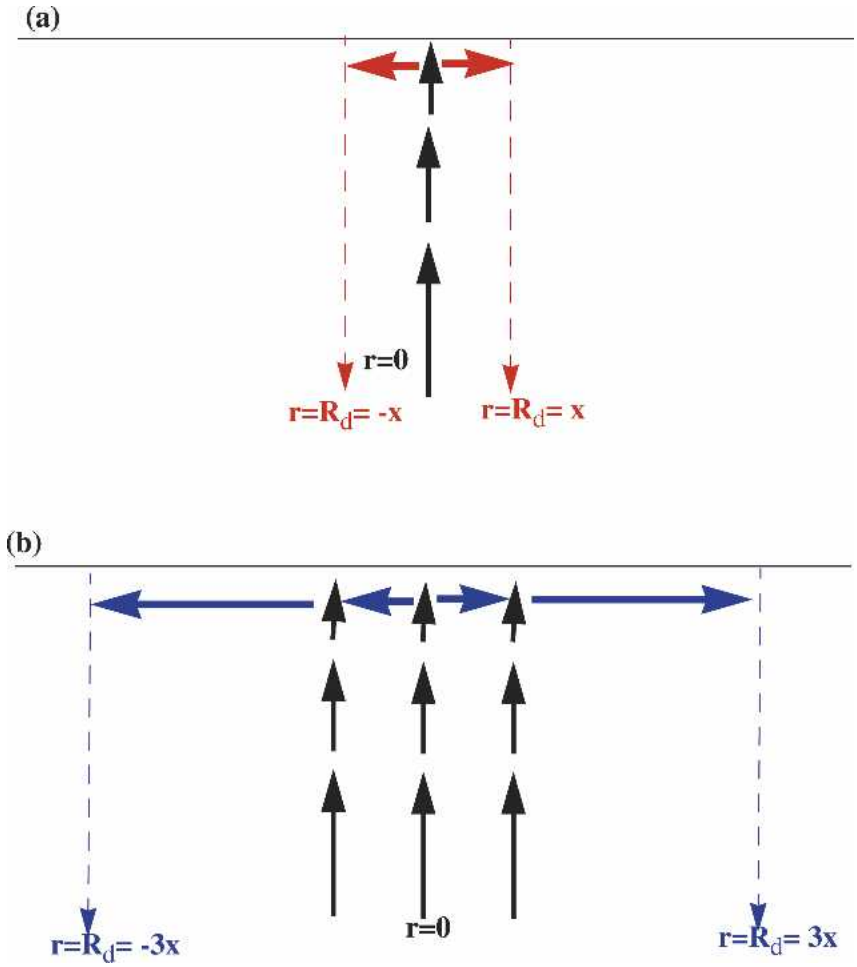

FIG. 2. Cartoon that shows the increase in v_r with radius as R_d increases. (a), (b) The length of the red and blue arrows indicate the magnitude of v_r. Here x can be any positive number.

$R_i(z)$ or R_o, we can determine the other using Eq. (1). The problem is that both $R_i(z)$ and R_o are actually unknown. We now present a method to determine R_o, keeping in mind that it must be independent of height. Our approach is based on the fact that, for given profiles of $w_i(z)$, $w_o(z)$, and $\sigma_i(z)$, the radial velocities will tend to increase as R_o increases [see Eq. (13) and Fig. 2]. This means that the area average of the large-eddy kinetic energy per unit mass in the horizontal part of the motion, $e_H = (1/2)\overline{v_r^2}$, will also tend to increase as R_o increases. Here the overbar denotes an area average over the whole horizontal cross section of the plume. These ideas suggest that we can determine R_o from e_H. We write

$$e_H = \frac{1}{\pi R_o^2}\int_0^{2\pi}\left(\int_0^{R_o}\frac{1}{2}v_r^2 r\,dr\right)d\phi = \frac{1}{R_o^2}\left(\int_0^{R_o} v_r^2 r\,dr\right). \quad (14)$$

Substituting the solution for $v_r(r)$ derived above and using (1), we find that

$$e_H = R_o^2\left\{\left[\frac{1}{4}\frac{\partial w_i}{\partial z}\right]^2\sigma^2 + \left[\frac{1}{2}\frac{\partial w_o}{\partial z}\right]^2 \times\left[-\frac{1}{2}\ln(\sigma) - (1-\sigma) + \frac{1}{4}(1-\sigma^2)\right]\right\}. \quad (15)$$

ADHOC2 predicts $(e_H)_M$, which is the vertical average of e_H through the depth of the PBL. Using this predicted (height independent) value of $(e_H)_M$, we can diagnose the (height independent) diameter of the plumes, R_o, from the vertical average of (15). We can then use (1) to diagnose $R_i(z)$, and solve for the two-dimensional distribution of the radial velocity using Eqs. (9)–(13). The kinematic structure of the plume is thus fully determined.

Using the LES model of Khairoutdinov and Randall

(2003), we performed a simulation of clear, weakly sheared convection on day 33 of the Wangara field experiments (Hicks 1978). Throughout this day, the evolution of the temperature and humidity profiles are typical of the very well-understood dry convective boundary layer (see, e.g., André et al. 1978). The simulation started at 0600 LT and ran for 12 simulated hours. We used horizontal and vertical resolutions of 100 and 40 m, respectively, with 75 levels and a horizontal domain of 64 × 64 grid cells. The time step was 2 s. We prescribed the surface latent and sensible heat fluxes from the observations (Hicks 1978).

To test Eq. (15) and the parameterized expressions for $v_r(r, z)$, we use the LES results for $\sigma_i(z)$, $(\partial w_i/\partial z)$, and $(\partial w_o/\partial z)$. In this calculation, w_i and w_o are the average vertical velocities over the regions where $w > 0$ and $w < 0$, respectively. Based on inspection of the LES results, the updrafts are assumed to be the inner cylinders. The fractional area $\sigma_i(z)$ is diagnosed, at each level, as the number of grid points where $w > 0$, divided by the total number of grid points. We vertically integrated Eq. (15) to obtain an expression for $(e_H)_M$ and R_o. We calculated $(e_H)_M$ from the LES and diagnosed the height-independent value of R_o by enforcing the vertical average of (15). This method yields $R_o = 1208$ m. We then calculated $R_i(z)$ using Eq. (1).

A second, independent estimate R_o can be obtained from the LES data. To do this, we conditionally sampled the LES fields at the height where the maximum vertical velocity occurs in the plume. Plume centers are identified as 3 × 3 block of grid cells where $w' > 1.5$ m s^{-1}. We then took averages over successively larger circles surrounding the plume centers and averaged over all plumes to get composite profiles of the vertical velocity as a function of distance from the center of an average plume. We correlated these averaged values with the plume center values. The results are shown in Fig. 3. Positive correlation coefficients indicate updrafts, while negative values show downdrafts. Figure 3 shows that $R_o = 1100$ m. This is encouragingly close to the first value diagnosed above.

We used our numerical results in Eqs. (9)–(13), with $R_o = 1208$ m, to determine the distribution of the radial velocity. The resulting radial and vertical velocities are depicted by the arrows plotted in Fig. 4. The longest arrows in the plot represent a particle speed of approximately 2 m s^{-1}. The dashed lines in the figure represent the height-dependent updraft–downdraft boundaries. The diagnosed radial velocity field shows convergence down low and divergence up high. Because R_i varies with z, we see a jump in v_r across the updraft–downdraft boundary [see Eq. (11)].

The results of the simulation were also used to test

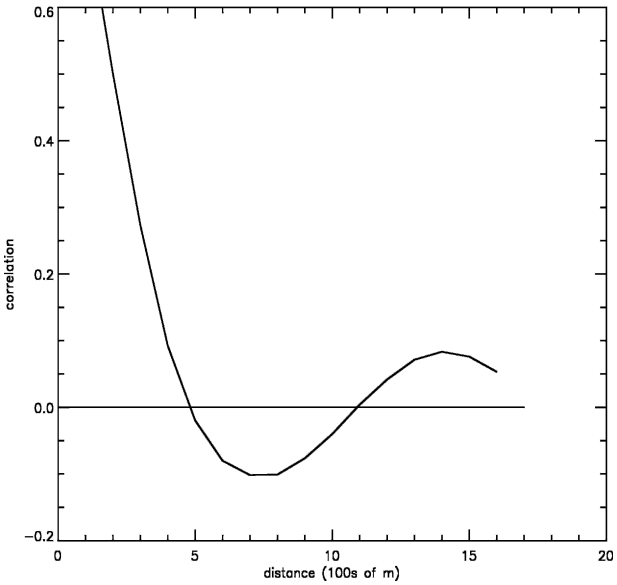

FIG. 3. The correlation coefficient of the average vertical velocities with the plume center velocities as a function of distance from the plume centers as calculated using LES data. Positive (negative) values indicate updraft (downdraft) regions.

Eq. (15). We used the LES value of $\sigma_i(z)$ in Eq. (1), to determine $R_i(z)$ for various values of R_o. We then used the LES values for $w_i(z)$ and $w_o(z)$ in Eq. (15) to calculate $e_H(z)$. In Fig. 5, the results are compared with the profile of e_H as diagnosed from the LES results. The best overall agreement near the surface and the top of the PBL occurs for $R_o = 900$ m, while the best agreement near the midlevel of the PBL is for $R_o = 1300$ m.

3. Rolls

We now consider idealized roll circulations, horizontally uniform in one direction. Our analysis of the rolls is broadly similar to that for plumes, as presented above. Key differences are that rolls are expected to occur in the presence of significant shear of the horizontal wind and they are expected to transport horizontal momentum vertically.

We simulated the roll case of Glendening (1996, hereafter G96) with the LES model described by Khairoutdinov and Randall (2003). All results in this section are compared with this LES run. In our simulated G96 LES case, we ran the model for 16 h with a domain size of 25 km × 18 km. The horizontal and vertical resolutions were 64 and 25 m, respectively. The time step was 2 s. The forcing parameters were designed to represent a sheared marine boundary layer with weak surface buoyancy below a strongly stable layer. We imposed a geostrophic wind of 15 m s^{-1} at an angle of 10° clockwise from the y axis. The surface fluxes were held con-

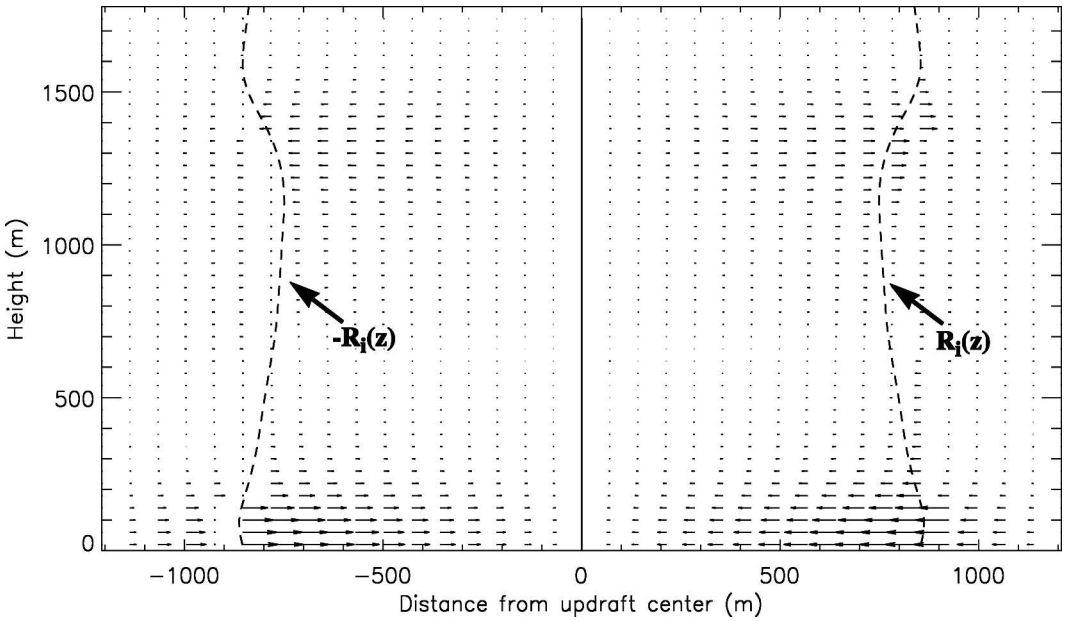

FIG. 4. Parameterized radial velocity obtained from Eqs. (9)–(13) for the Wangara case. The solid line is the updraft center, while the dashed lines represent the updraft–downdraft border. The longest arrows shown (near the bottom) are approximately 2.0 m s^{-1}.

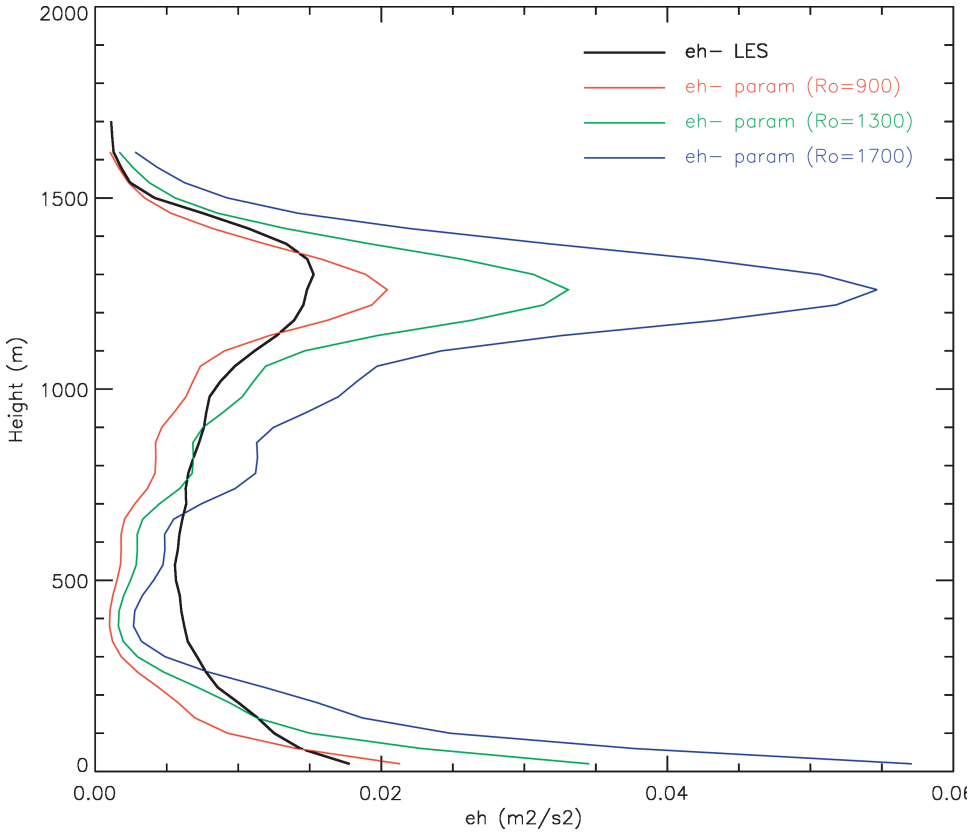

FIG. 5. Comparison of the LES and parameterized [Eq. (15)] horizontal TKE for different values of R_o.

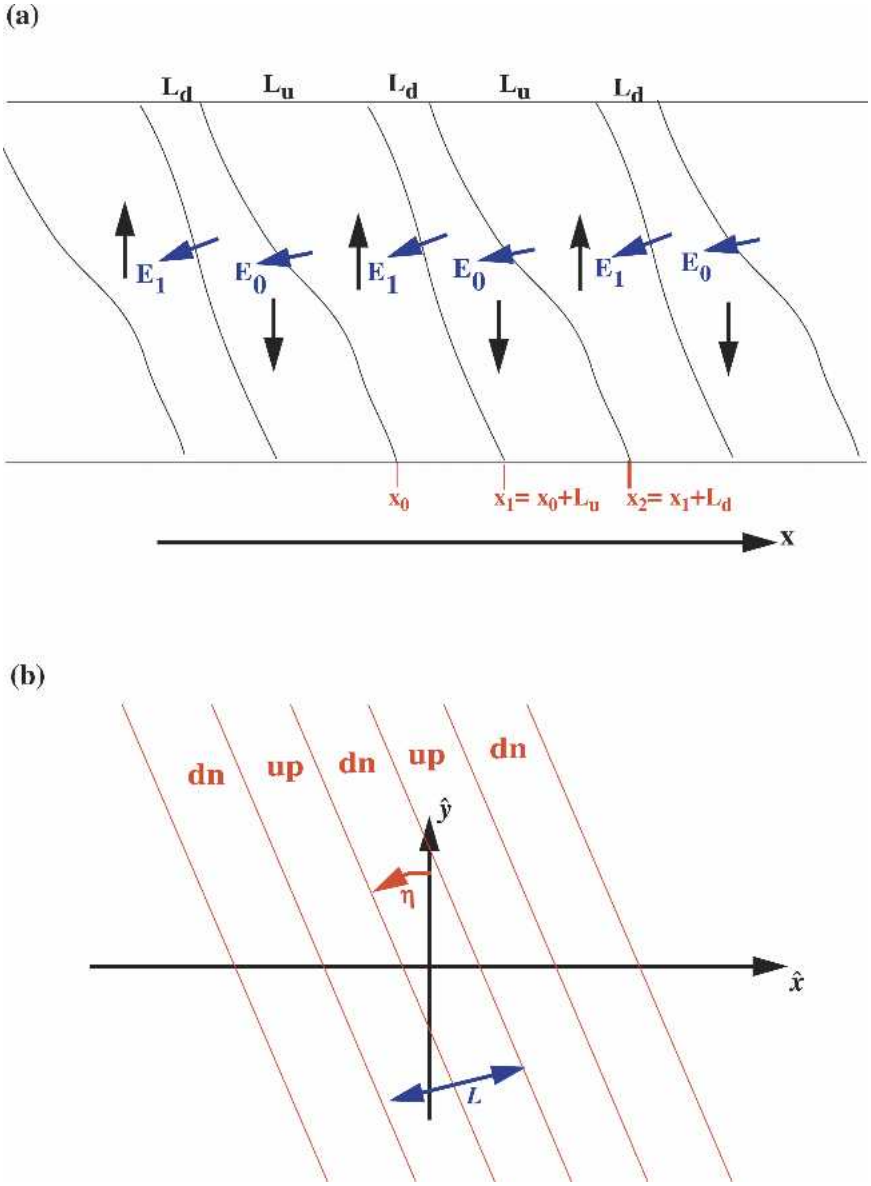

FIG. 6. Cross sections through the roll: (a) vertical cross sections L_u and L_d are the widths of the updraft and downdraft, respectively, while E_0 and E_1 represent mass entrained from the updraft to the downdraft and vice versa, respectively. Black arrows show the updrafts and downdrafts while blue arrows show lateral mass fluxes. The directions of the blue arrows merely indicate the sign conventions for these mass fluxes and are not meant to depict the actual pattern of mass flow. (b) Horizontal cross section: the $(\hat{x}, \hat{y})$ coordinates are west-to-east and south-to-north, respectively. The rolls are invariant along the direction that makes an angle η with the $\hat{y}$ axis. We call this the y direction so that $\partial/\partial y = 0$.

stant at $(\overline{w'u'})_s = 221\ \mathrm{m^2\ s^{-2}}$; $(\overline{w'\theta'})_s = 0.134\ \mathrm{K\ m\ s^{-1}}$; and $(\overline{w'q'})_s = 0.076\ \mathrm{g\ m\ s^{-1}\ kg^{-1}}$. The temperature and humidity fluxes were chosen so as to contribute equally to the total buoyancy flux, $(\overline{w'\theta_v'})_s = 0.264\ \mathrm{K\ m\ s^{-1}}$. To attenuate the boundary layer growth rate, a base-state stratification of $\partial\theta/\partial z = 10\ \mathrm{K\ km^{-1}}$ is chosen above the boundary layer. In our results, the length scale of the along-roll variations is approximately 4 times the cross-roll length scale, as found by G96. The results of the simulation will be used later.

To construct our idealized model of a field of rolls, we adopt Cartesian coordinates $(\hat{x}, \hat{y})$, and assume alternating updrafts and downdrafts, aligned at an angle η from the $\hat{y}$ axis (see Figs. 6a,b). For convenience, we

define a rotated coordinate system (x, y), such that $\partial\cdot/\partial y = 0$; we also define a corresponding x direction, which is oriented at the same angle η with respect to the $\hat{x}$ axis. The horizontal velocity components are (u, v) in the (x, y) system, and $(\hat{u}, \hat{v})$ in the $(\hat{x}, \hat{y})$ system. We assume that the horizontal averages of $\hat{u}$ and $\hat{v}$ are known as functions of height. A method to determine η is presented in the next section.

Let $x = x_0(z)$ denote the boundary between one particular downdraft and one particular updraft with the updraft on the side of the larger values of x (Fig. 6a). The opposite wall of the updraft is at $x = x_0(z) + L_u(z) \equiv x_1(z)$ so that the updraft has width $L_u(z) = x_1(z) - x_0(z)$, and occupies the region $x_0(z) < x < x_1(z)$. A neighboring downdraft occupies the region $x_1(z) < x < x_0(z) + L = x_1(z) + L_d(z) \equiv x_2$, where L is the total width of the roll; that is,

$$L = L_u + L_d, \tag{16}$$

and $L_d(z)$ is the width of the downdraft. The fractional area occupied by the updraft is

$$\sigma(z) = \frac{L_u(z)}{L} = \frac{x_1(z) - x_0(z)}{L}. \tag{17}$$

We assume that

$$\frac{\partial L}{\partial z} = 0. \tag{18}$$

Because L is the total width of a roll and R_o is the radius of a plume, the assumption that L is independent of height is analogous to our earlier assumption that R_o is independent of height. From (17) and (18), we see that

$$\frac{\partial x_1}{\partial z} - \frac{\partial x_0}{\partial z} = L\frac{\partial \sigma}{\partial z}. \tag{19}$$

This will be used later.

The Bousinesq version of the continuity equation can be written in the (x, y) system as

$$\frac{\partial u}{\partial x} + \frac{\partial w}{\partial z} = 0, \tag{20}$$

The assumption that $\partial/\partial y = 0$ has been used in writing (20). To determine the spatial distribution of u, using the continuity equation, we start arbitrarily at $x = x_0 + \varepsilon$ and integrate (20) with respect to x (across the updraft) to $x = x_1 - \varepsilon$ to obtain

$$u(x) = u(x_0 + \varepsilon) - (x - x_0)\frac{\partial w_u}{\partial z} \quad \text{for} \quad x_0 < x < x_1. \tag{21}$$

The mass flow rates must be continuous across $x = x_0$ and $x = x_1$. This implies that

$$w_u\frac{\partial x_0}{\partial z} - u_{x_0+\varepsilon} = w_d\frac{\partial x_0}{\partial z} - u_{x_0-\varepsilon}, \tag{22}$$

$$w_d\frac{\partial x_1}{\partial z} - u_{x_1+\varepsilon} = w_u\frac{\partial x_1}{\partial z} - u_{x_1-\varepsilon}. \tag{23}$$

In Eqs. (22)–(23), $()_u$ denotes an average over the updraft $[x_0(z) < x < x_1]$; $()_d$ denotes an average over the downdraft $(x_1(z) < x < x_2)$; $()_{x_0+\varepsilon}$, $()_{x_0-\varepsilon}$, $()_{x_1+\varepsilon}$, and $()_{x_1-\varepsilon}$ denote values evaluated just to the right and left of $x = x_0$ and $x = x_1$, respectively (see Fig. 6a). Use of (17) and (23) allows us to write

$$u(x_1 + \varepsilon) = u(x_0 + \varepsilon) - L_u\frac{\partial w_u}{\partial z} - (w_u - w_d)\frac{\partial x_1}{\partial z}. \tag{24}$$

Further integration of (20) then gives

$$u(x) = u(x_0 + \varepsilon) - L_u\frac{\partial w_u}{\partial z} - (w_u - w_d)\frac{\partial x_1}{\partial z} - (x - x_1)\frac{\partial w_d}{\partial z} \quad \text{for} \quad x_1 < x < x_2. \tag{25}$$

Equations (21) and (25) determine $u(x)$ throughout a roll except at the boundaries ($x = x_0$, $x = x_1$, and $x = x_2$). If the boundaries between the updraft and downdraft are not tilted, then $u(x)$ is continuous there. If the boundaries are tilted, then $u(x)$ is discontinuous there.

It is useful to rewrite (21) and (25) as

$$u(x) = u(x_0 + \varepsilon) - \left(\frac{x - x_0}{L}\right)\left\{L_d\frac{\partial}{\partial z}(w_u - w_d) - (w_u - w_d)\frac{\partial}{\partial z}(x_1 - x_0)\right\} \quad \text{for} \quad x_0 < x < x_1, \tag{26}$$

$$u(x) = u(x_0 + \varepsilon) + \left\{\frac{L_u[-L_d + (x - x_1)]}{L}\right\}\frac{\partial}{\partial z} \times (w_u - w_d) + (w_u - w_d)\left\{\frac{\partial x_1}{\partial z}\left[\frac{-L_d + (x - x_1)}{L}\right] + \frac{\partial x_0}{\partial z}\left[\frac{-L_u - (x - x_1)}{L}\right]\right\} \quad \text{for} \quad x_1 < x < x_2, \tag{27}$$

respectively. In deriving (26) and (27), we have used $\overline{w} = 0$.

The next step is to work out u', the departure of u from its horizontal average, $\overline{u}$. Integration gives

$$\overline{u} = \frac{1}{L}\int_{x_0}^{x_0+L} u\,dx = \frac{1}{L}\left(\int_{x_0}^{x_0+L_u} u\,dx + \int_{x_1}^{x_1+L_d} u\,dx\right)$$
$$= u(x_0+\varepsilon) - \left(\frac{L_u L_d}{2L}\right)\frac{\partial}{\partial z}(w_u - w_d) + \left(\frac{w_u - w_d}{2}\right)$$
$$\times\left[\frac{\partial x_1}{\partial z}\left(\frac{L_u - L_d}{L}\right) - \frac{\partial x_0}{\partial z}\right]. \quad (28)$$

Equation (28) can be used to eliminate $u(x_0 + \varepsilon)$ in favor of $\overline{u}$. With this substitution, (26) and (27) can be rewritten as

$$u' = \frac{L_d}{L}\left(\frac{L_u}{2}\right)\frac{\partial}{\partial z}(w_u - w_d) + \frac{(w_u - w_d)}{2}$$
$$\times\left[\left(\frac{\partial x_0}{\partial z}\right) - \left(\frac{\partial x_1}{\partial z}\right)\left(\frac{L_u - L_d}{L}\right)\right] + \left(\frac{x - x_0}{L}\right)$$
$$\times\left\{-L_d\frac{\partial}{\partial z}(w_u - w_d) + (w_u - w_d)\right.$$
$$\left.\times\left(\frac{\partial x_1}{\partial z} - \frac{\partial x_0}{\partial z}\right)\right\} \quad \text{for} \quad x_0 < x < x_1, \quad (29)$$

and

$$u' = -\left(\frac{L_u}{L}\right)\left(\frac{L_d}{2}\right)\frac{\partial}{\partial z}(w_u - w_d) + (w_u - w_d)$$
$$\times\left[\left(\frac{1}{2} - \frac{L_u}{L}\right)\left(\frac{\partial x_0}{\partial z}\right) - \frac{1}{2}\left(\frac{\partial x_1}{\partial z}\right)\right] + \left(\frac{x - x_1}{L}\right)$$
$$\times\left\{L_u\frac{\partial}{\partial z}(w_u - w_d) + (w_u - w_d)\right.$$
$$\left.\times\left(\frac{\partial x_1}{\partial z} - \frac{\partial x_0}{\partial z}\right)\right\} \quad \text{for} \quad x_1 < x < x_2, \quad (30)$$

respectively, where

$$u' \equiv u(x) - \overline{u}. \quad (31)$$

We can now compute moments involving u'. For example, the variance of the u wind can be written as

$$\overline{u'^2} = \frac{1}{L}\int_{x_0}^{x_0+L} u'^2\,dx$$
$$= \frac{1}{L}\left(\int_{x_0}^{x_0+L_u} u'^2\,dx + \int_{x_1}^{x_1+L_d} u'^2\,dx\right). \quad (32)$$

After substituting from (29) and (30) and performing a lengthy algebraic exercise which is detailed in the appendix, we obtain

$$\overline{u'u'} = \frac{1}{3}(LD)^2 + \frac{2L}{3}D\left[(1-2\sigma)\left(\frac{\partial x_1}{\partial z} - \frac{\partial x_0}{\partial z}\right)\right.$$
$$\left. + 2\sigma(1-\sigma)\left(\frac{\partial x_0}{\partial z} + \frac{\partial x_1}{\partial z}\right)\right](w_u - w_d)$$
$$+ (w_u - w_d)^2\left\{\frac{1}{2}\sigma(1-\sigma)\left(\frac{\partial x_0}{\partial z} + \frac{\partial x_1}{\partial z}\right)\right.$$
$$\left.\times\left[\sigma\frac{\partial x_0}{\partial z} + (1-\sigma)\frac{\partial x_1}{\partial z}\right]\right\} + (w_u - w_d)^2$$
$$\times\left(\frac{\partial x_1}{\partial z} - \frac{\partial x_0}{\partial z}\right)^2\left(\frac{1 - 3\sigma + 3\sigma^2}{3}\right), \quad (33)$$

where for convenience, we define

$$D \equiv \sigma(1-\sigma)\frac{\partial}{\partial z}(w_u - w_d). \quad (34)$$

Equation (33) will be further simplified below, and tested against the LES results.

As shown in the appendix, the vertical flux of u momentum is given by

$$\overline{w'u'} = \frac{1}{L}\left(\int_{x_0}^{x_0+L_u} w_u u'\,dx + \int_{x_1}^{x_1+L_d} w_d u'\,dx\right)$$
$$= (w_u - w_d)^2\left(\frac{L_u L_d}{2L^2}\right)\left[\left(\frac{\partial x_0}{\partial z}\right) + \left(\frac{\partial x_1}{\partial z}\right)\right]$$
$$= (w_u - w_d)^2\sigma(1-\sigma)\lambda. \quad (35)$$

According to (35), the momentum flux is different from zero only when the tilt of the updrafts and downdrafts, defined by

$$\lambda \equiv \frac{1}{2}\left[\left(\frac{\partial x_0}{\partial z}\right) + \left(\frac{\partial x_1}{\partial z}\right)\right], \quad (36)$$

is different from zero. Comparing (35) and (3), we see that

$$\overline{w'u'} = (\overline{w'w'})\lambda. \quad (37)$$

Also, use of (19) and (34)–(36) allows us to simplify (33) to

$$\overline{u'u'} = \frac{1}{3}(LD)^2 + \frac{2LD}{3}\left[(1-2\sigma)\left(L\frac{\partial\sigma}{\partial z}\right)\right.$$
$$\left. + 4\sigma(1-\sigma)\lambda\right](w_u - w_d)$$
$$+ \overline{w'u'}\left[\lambda + \left(\frac{1-2\sigma}{2}\right)L\frac{\partial\sigma}{\partial z}\right]$$
$$+ (w_u - w_d)^2\left(L\frac{\partial\sigma}{\partial z}\right)^2\left(\frac{1 - 3\sigma + 3\sigma^2}{3}\right). \quad (38)$$

Using (36) and (19), we obtain

$$\frac{\partial x_0}{\partial z} = \lambda - \frac{L}{2}\frac{\partial \sigma}{\partial z}, \tag{39}$$

and

$$\frac{\partial x_1}{\partial z} = \lambda + \frac{L}{2}\frac{\partial \sigma}{\partial z}. \tag{40}$$

If L, $\sigma(z)$, $\overline{w'u'}$ and $\overline{w'w'}$ are known, we can diagnose $(\partial x_0/\partial z)$ and $(\partial x_1/\partial z)$ from (39) and (40).

The values of $\overline{w'u'}$, $\overline{w'w'}$, and σ can readily be obtained from the LES. We also use the LES to diagnose L, as follows. We examine a horizontal slice through the LES data at the height of the maximum vertical velocity (in the example given below, at $z = 300$ m). We compute the autocorrelations of vertical velocity across the domain along lines whose angles with the y axis (the axis of mean wind) ranged from $-15°$ to $15°$. The highest correlation was found for an angle of 8° to the left of the mean wind. We then averaged the vertical velocity across the domain along all lines with this orientation. This averaged cross-roll vertical velocity is shown in Fig. 7 for a section of the domain that covers two rolls. By inspection, L (indicated by an updraft–downdraft pair) is about 3600 m. Section 4 presents an analytical method to determine L.

Using the LES-diagnosed values of L, $\overline{w'u'}$, $\overline{w'w'}$, and σ, we can determine the tilt. The results are plotted in Fig. 8. In the figure, $(\partial x_0/\partial z)$ is the tilt of the updraft–downdraft wall to the left side of the updraft, while $(\partial x_1/\partial z)$ is the tilt of the analogous wall on the right side of the updraft (see Fig. 6). The two sides of the updraft tilt in opposite directions. The tilt ranges between 0% and 10% throughout the PBL. Plots of observed and numerically simulated rolls show this to be a reasonable number (G96; Etling and Brown 1993).

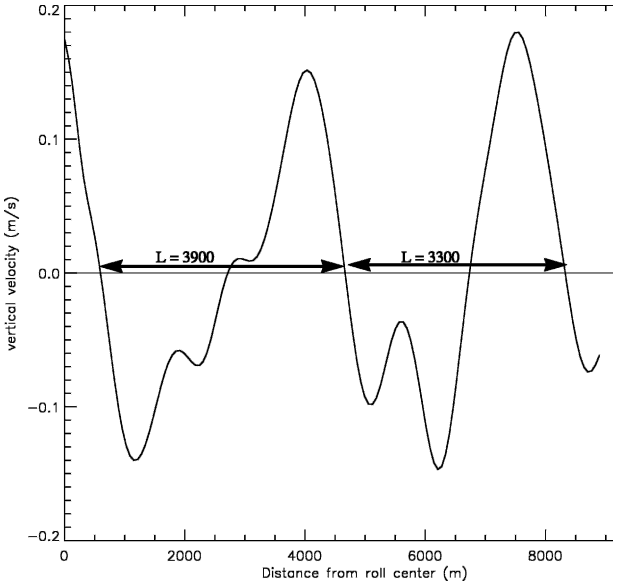

FIG. 7. Average vertical velocity as a function distance from a roll center. Adjacent positive and negative regions show a complete roll formation. The length of the two rolls shown is indicated by the arrows.

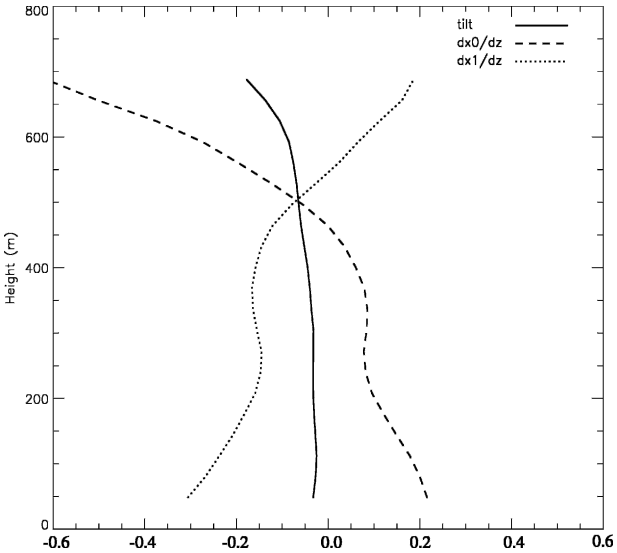

FIG. 8. Average tilt of the roll; $(\partial x_0/\partial z)$ is the tilt of the updraft–downdraft wall to the left side of the updraft, while $(\partial x_1/\partial z)$ is the tilt of the analogous wall on the right side of the updraft (see Fig. 6). The curve labeled tilt is the average tilt of the roll.

At this point, we have a complete picture of the roll's size, shape including tilt, and circulation. We can use Eqs. (21)–(25), along with the filtered LES updraft and downdraft vertical velocities, to get the total wind vector. Figure 9 shows the diagnosed roll structure.

Figure 10a shows $\overline{u'u'}$ as diagnosed from (33) and as determined directly from the LES. In Fig. 10b, we show the contributions to the diagnosed value of $\overline{u'u'}$ from the first, second, and third lines of Eq. (33). The shape and maximum values of $\overline{u'u'}$ are well represented by the parameterization. As with the Wangara plumes, however, the diagnosed $\overline{u'u'}$ is too small in the PBL midlevels, and slightly too large near the PBL top and near the surface. The reason for the unrealistically small values of $\overline{u'u'}$ at midlevels may be our neglect of smaller-scale eddies, a known limitation of the mass-flux approach. Figure 10b shows that, for this particular simulation diagnosed here, the first line of (33) is strongly dominant.

Similar methods can be used to work out statistics involving v'. Unlike u', v' is independent of x inside the

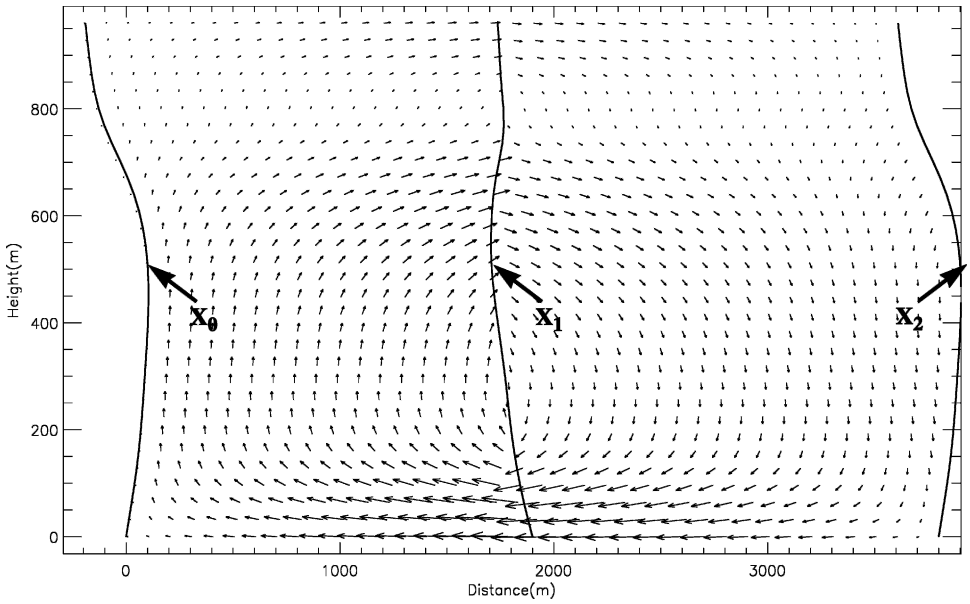

FIG. 9. Picture of the parameterized roll and its parameterized circulation. The horizontal component of the roll circulation is given by Eqs. (21)–(25). The vertical component is calculated from the LES updraft and downdraft velocities. The tilt of the roll can be seen by the lines indicating the $x_0(z)$, $x_1(z)$, and $x_2(z)$ boundaries calculated in section 3 and drawn in Fig. 8.

updraft, and also inside the downdraft.[2] It is also independent of y, of course, so that we can define v_u and v_d as functions of z only. In this respect v' is similar to w', and, in fact, v' and w' are perfectly correlated in our idealized model (in the case of the rolls, this correlation is actually negative). The simplest results are

$$\overline{v'^2} = \sigma(1-\sigma)(v_u - v_d)^2, \tag{41}$$

which is analogous to (3), and

$$\overline{w'v'} = \sigma(1-\sigma)(w_u - w_d)(v_u - v_d), \tag{42}$$

where v_u and v_d are the x- (and y-) independent values of v in the updraft and downdraft, respectively. Figure 11 shows a comparison of the parameterized lateral and longitudinal momentum fluxes [Eqs. (35) and (42), respectively] with those diagnosed from LES. We see that, despite our somewhat crude assumption that v is independent of x within the updraft and downdraft, the results are in reasonable agreement with the LES results. The larger differences near the top and bottom are presumably associated with subplume-scale fluxes, which become important at those levels.

[2] This directly follows from the assumption that w is independent of x in the updraft and downdraft. The main source of v' is vertical advection of $\bar{v}$ by w'. Therefore, if w' is independent of x, then $\partial v'/\partial t$ will also be independent of x, and so will v'. See also Fig. 11, discussed below.

Comparing (41) and (42), and using (3), we see that

$$\overline{v'^2} = \frac{(\overline{w'v'})^2}{\overline{w'w'}}. \tag{43}$$

This will be used below, to determine η.

The analysis for $\overline{u'v'}$ is very similar to that for $\overline{w'u'}$. By analogy with (35), we have

$$\overline{u'v'} = (w_u - w_d)(v_u - v_d)\left(\frac{L_u L_d}{L^2}\right)\lambda. \tag{44}$$

Equation (44) can be rewritten as

$$\overline{u'v'} = (\overline{w'v'})\lambda. \tag{45}$$

4. Solving for the orientation angle, tilt, and wavelength

In our earlier analysis of unsheared plumes, we presented a method to determine R_o, the plume radius. The approach was to choose the value of R_o so that the vertically averaged value of e_H, as diagnosed from the continuity equation and the vertical motion, agreed with the corresponding value prognosed by ADHOC. We take a similar approach to the corresponding problem of determining L, the wavelength of the rolls. A major complication, however, is that the roll equations involve additional parameters, namely, the orientation angle, η, and the tilts $\partial x_0/\partial z$ and $\partial x_1/\partial z$.

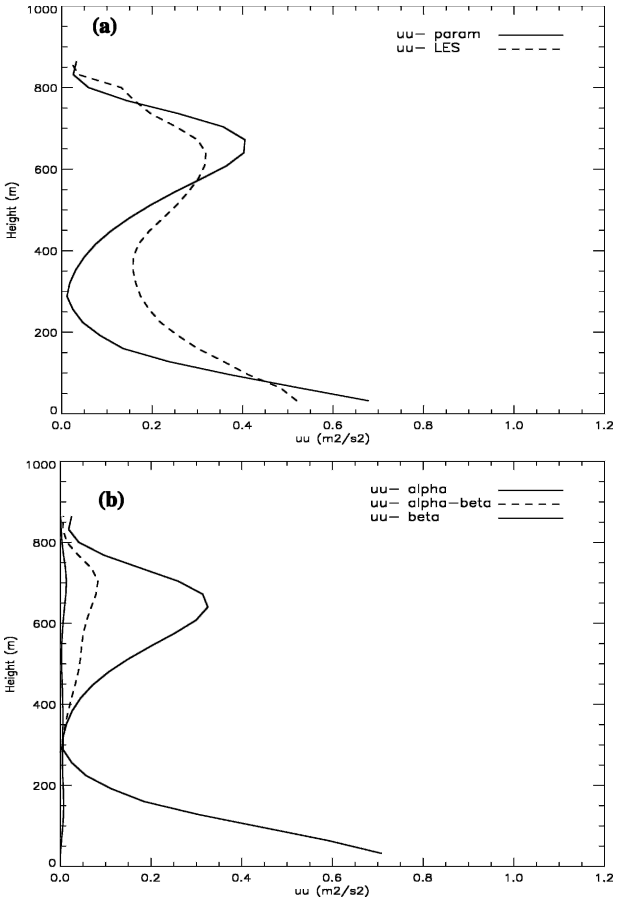

FIG. 10. (a) Comparison of the parameterized $\overline{u'u'}$, as given by (33), to that of the LES for the Glendening (1996) roll case. (b) Contributions to $\overline{u'u'}$ from the first, second, and third lines of (33).

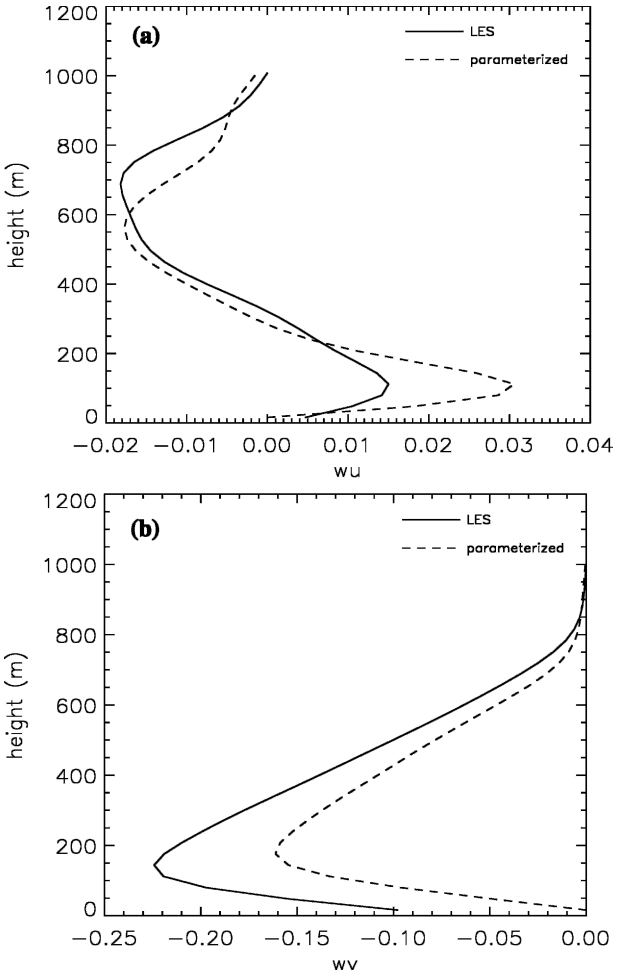

FIG. 11. Comparison of the parameterized (a) lateral momentum fluxes $\overline{w'u'}$ [given by Eq. (35)] and (b) longitudinal momentum fluxes $\overline{w'v'}$ [given by Eq. (42)] with those diagnosed from LES.

First consider the orientation angle, η. We can write

$$\overline{w'u'} = \overline{w'(\hat{u})'}\cos\eta + \overline{w'(\hat{v})'}\sin\eta, \tag{46}$$

$$\overline{w'v'} = -\overline{w'(\hat{u})'}\sin\eta + \overline{w'(\hat{v})'}\cos\eta, \tag{47}$$

$$\overline{u'u'} = \overline{[(\hat{u})'\cos\eta + (\hat{v})'\sin\eta]^2} = \overline{(\hat{u})'^2}\cos^2\eta + 2\overline{(\hat{u})'(\hat{v})'}\cos\eta\sin\eta + \overline{(\hat{v})'^2}\sin^2\eta, \tag{48}$$

$$\overline{v'v'} = \overline{[-(\hat{u})'\sin\eta + (\hat{v})'\cos\eta]^2} = \overline{(\hat{u})'^2}\sin^2\eta - 2\overline{(\hat{u})'(\hat{v})'}\cos\eta\sin\eta + \overline{(\hat{v})'^2}\cos^2\eta, \tag{49}$$

$$\overline{u'v'} = \overline{[(\hat{u})'\cos\eta + (\hat{v})'\sin\eta][-(\hat{u})'\sin\eta + (\hat{v})'\cos\eta]} = -[\overline{(\hat{v})'^2} - \overline{(\hat{u})'^2}]\cos\eta\sin\eta + \overline{(\hat{u})'(\hat{v})'}(\cos^2\eta - \sin^2\eta) = -[\overline{(\hat{v})'^2} - \overline{(\hat{u})'^2}]\frac{\sin2\eta}{2} + \overline{(\hat{u})'(\hat{v})'}\cos2\eta. \tag{50}$$

Suppose that, except for η, all quantities on the right-hand sides of (46)–(50) were known, for example, via prediction by ADHOC2. In the preceding section, we have used the idealized roll model to derive several relationships among the quantities on the left-hand sides of (46)–(50). A proper choice of η is needed to ensure that these relationships are actually satisfied. In particular, substitution of (47) and (49) into (43) gives

$$\overline{(\hat{u})'^2}\sin^2\eta - 2\overline{(\hat{u})'(\hat{v})'}\cos\eta\sin\eta + \overline{(\hat{v})'^2}\cos^2\eta = \frac{\{-\overline{w'(\hat{u})'}\sin\eta + \overline{w'(\hat{v})'}\cos\eta\}^2}{\overline{w'w'}}. \tag{51}$$

Vertical averaging of both sides of (51) through the depth of the PBL gives, after some rearrangement,

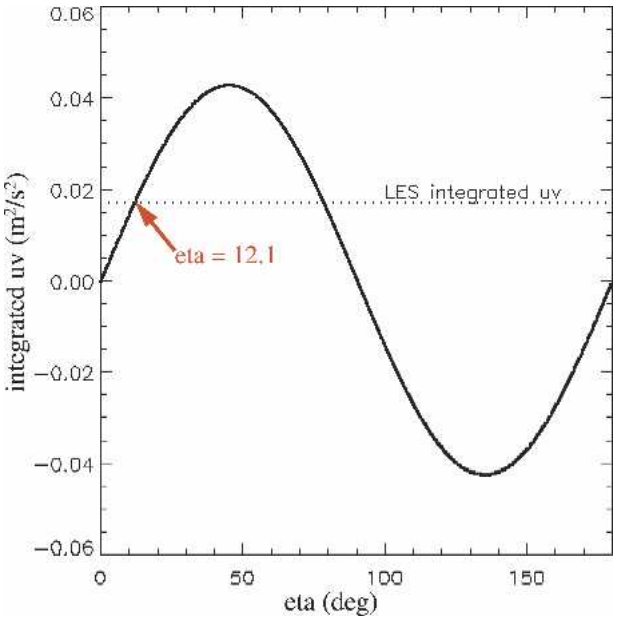

FIG. 12. Graphical solution for η. The intersection of the LES-integrated value of $\overline{u'v'}$ (dotted line) with the curve of the integrated value of $\overline{u'v'}$ found for different values of η (solid line) is the solution. This occurs at $\eta = 12.1°$ and at $\eta = 78.6°$. The former is chosen because it maximizes the vertically integrated shear production.

$$\left\{\overline{(\hat{u})'^2} - \frac{\overline{w'(\hat{u})'^2}}{\overline{w'w'}}\right\}_M \sin^2\eta - 2\left\{\overline{(\hat{u})'(\hat{v})'} - \frac{[\overline{w'(\hat{u})'}][\overline{w'(\hat{v})'}]}{\overline{w'w'}}\right\}_M \cos\eta\sin\eta + \left\{\overline{(\hat{v})'^2} - \frac{\overline{w'(\hat{v})'^2}}{\overline{w'w'}}\right\}_M \cos^2\eta = 0. \quad (52)$$

Here we have used our assumption that η is independent of height.

Equation (52) can be solved for η, provided that the various vertically averaged quantities under the curly brackets are known. The roll version of ADHOC2 predicts $[\overline{(\hat{u})'^2}]_M$, $[\overline{(\hat{u})'(\hat{v})'}]_M$, and $[\overline{(\hat{v})'^2}]_M$. It also predicts $\overline{w'w'}$, $\overline{w'(\hat{u})'}$, and $\overline{w'(\hat{v})'}$ as functions of height so that the additional vertically averaged quantities within the braces of (52) can be evaluated, leaving η as the only unknown. In this way, ADHOC2 determines the value of η.

Note that there are some realizability issues here, since at each height we must require that $|\overline{w'(\hat{u})'}|^2 \le \overline{(\hat{u})'^2}\,\overline{w'w'}$, and a similar inequality for the $\hat{v}$ component.

For the plume version of ADHOC2, the momentum fluxes are known as functions of height because they are simply equal to zero at all heights. For the roll version of ADHOC2, the momentum fluxes are predicted as functions of height. For the plumes, we predict $(e_H)_M$, which is analogous to predicting $\overline{(\hat{u})'^2}_M$, $\overline{(\hat{v})'^2}_M$, and $[\overline{(\hat{u})'(\hat{v})'}]_M$ for the rolls. The plume and roll versions of ADHOC2 thus have parallel structures.

A diagnostic example based on analysis of LES results is shown in Fig. 12. The solution is given by the intersection of the LES-integrated value for $\overline{u'v'}$ and the curve given by determining $(\overline{u'v'})_M$ for different values of η. There are two solutions, at $\eta = 12.1°$ and $\eta = 78.6°$. We choose the former because it maximizes the vertically integrated rate of turbulence kinetic energy (TKE) production through the shear term. This solution is reasonably close to the value diagnosed earlier ($\eta = 8°$) using the autocorrelation method.

Once η has been determined, we can diagnose $\overline{w'u'}(z)$ and $\overline{w'v'}(z)$ from (46) and (47), respectively; $\overline{v'^2}(z)$ from (43); and $\lambda(z)$ from (37). We could also determine $\partial x_0/\partial z$ and $\partial x_1/\partial z$ from (39) and (40), if we knew the value of L. The last major task is to determine L, which we can do by using (38). Collecting powers of L in (38), we obtain

$$0 = L^2\left\{\frac{D^2}{3}\left[1 + 2(1-2\sigma)\frac{\partial\sigma}{\partial z}\right] + (w_u - w_d)^2\left(\frac{\partial\sigma}{\partial z}\right)^2 \times \left(\frac{1 - 3\sigma + 3\sigma^2}{3}\right)\right\} + L\left[\frac{2D}{3}4\sigma(1-\sigma)\lambda(w_u - w_d) + \overline{w'u'}\left(\frac{1-2\sigma}{2}\right)\frac{\partial\sigma}{\partial z}\right] + (\overline{w'u'}\lambda - \overline{u'u'}). \quad (53)$$

We vertically average this equation through the depth of the PBL, using our assumption that L is independent of height. The result can be solved as a quadratic equation for L. Using the LES data, we get $L = 2988$ m. This is close to the value obtained using autocorrelation (Fig. 7).

5. Summary and discussion

In this paper, we describe a new method to represent momentum fluxes and variances in a PBL mass-flux model. Our approach is based on the assumption that coherent structures, that is, plumes or rolls, dominate the PBL physics. Rolls occur with shear and produce vertical momentum transport, while the plumes occur in the absence of shear and do not transport momentum.

Using idealized models of plumes and rolls, we developed expressions for the velocity variances and covariances. These results have been tested using LES data from simulations of the clear convective Wangara

experiments and a roll case described by Glendening (1996).

The parameterizations presented here have been designed to work in a mass-flux model called ADHOC (Lappen and Randall 2001a–c). The original version of ADHOC predicted the fractional area covered by rising motion, as well as moments of the thermodynamic variables and the vertical velocity, including of course the vertical fluxes of the thermodynamic energy and moisture.

The newest version, ADHOC2, is based on the ideas presented here, and predicts second moments involving the horizontal velocity. The plume version of ADHOC2 predicts $(e_H)_M$, and the roll version predicts $(\overline{u'u'})_M$, $(\overline{v'v'})_M$, and $(\overline{u'v'})_M$. We use the continuity equation to develop expressions for the horizontal velocity components. These are then used to derive expressions for second moments involving the horizontal velocity components.

In the plume version of ADHOC2, the expression for $(e_H)_M$ involves the outer radius of the plumes, R_0. We present a method to determine R_0 from the predicted value of $(e_H)_M$. Once R_0 is known, we can diagnose the height-dependent radius of the inner cylinder, $R_i(z)$, using $\sigma 7(z)$. This describes the size and shape of the convective plume, as well as its circulation. We applied this to the Wangara case (Hicks 1978) and the resulting plume (sketched in Fig. 4) looks as expected. This is the first time (to our knowledge) that a simple PBL model has been able to diagnose such structures. We found that $R_0 = 1208$ m. To check this value, we used LES data for the Wangara case and compared the parameterized values of e_h to those simulated by the LES for different values of R_0. The closest agreement was found for R_0 values close to that diagnosed by our parameterization. Further confirmation of the validity of our diagnosed R_0 value came from conditionally averaging the LES plumes to get a composite vertical velocity as a function of distance from the plume center. Correlation of these velocities with the plume center values gave $R_0 = 1100$ m.

In the roll version of ADHOC2, the expressions for the second moments involving the horizontal velocity components depend on the widths of the updraft and downdraft, L_u and L_d, the tilts of the updraft/downdraft walls, $\partial x_0/\partial z$ and $\partial x_1/\partial z$ and the orientation angle, η. As in the plume version, the continuity equation was integrated to derive expressions for second moments involving the horizontal velocity components. The orientation angle can be determined from Eq. (52) using the predicted values of $\overline{w'u'}$, $\overline{w'v'}$, and $\overline{w'w'}$, as well as the predicted vertically averaged covariance $(\overline{u'v'})_M$. Once η is known, L can be calculated using (53). Finally, L_u, L_d, and the tilt of the updraft/downdraft wall can be determined using Eqs. (17), (39), and (40). Using the LES data, our parameterization gives $\eta = 12.1°$. Plotting the LES rolls directly using an autocorrelation technique gave a value of about $\eta = 8°$, close to our parameterized value. For L, the agreement was fair. Our parameterization yielded $L = 2988$ m, while inspection of the roll using autocorrelation showed the value to be closer to $L = 3600$ m. This is the first time (to our knowledge) that a PBL model has been able to diagnose the tilt, orientation angle, and wavelength of a field of rolls. In the future, we will test this parameterization on rolls with differing aspect ratios and surface buoyancy fluxes.

In our companion paper (Lappen and Randall 2005, manuscript submitted to *J. Atmos. Sci.*), we present methods to diagnose the pressure terms in the higher moment momentum equations using these assumed geometries and the available mass-flux quantities. Prior to the present study, PBL mass-flux models have been used to diagnose only the thermodynamic properties of convection. The methods presented here and in our companion paper permit mass-flux models of the PBL to determine the corresponding statistics for the involving the horizontal wind components.

A major limitation of our approach is that the geometries of the circulations are highly idealized. It remains to be seen how well our approach will work for a wide range of realistic conditions.

Acknowledgments. This research was funded by the National Science Foundation under Grant ATM-9812384, and by the U.S. Department of Energy under Cooperative Agreement DE-FC02-01ER63163, both to Colorado State University.

APPENDIX

Calculation of Higher Moments for Roll Case

a. $\overline{u'u'}$

Equations (29) and (30) can be written schematically as

$$u' = A + \left(\frac{x - x_0}{L}\right)B \quad \text{for} \quad x_0 < x < x_1, \quad \text{(A1)}$$

$$u' = C + \left(\frac{x - x_1}{L}\right)D \quad \text{for} \quad x_1 < x < x_2, \quad \text{(A2)}$$

where A, B, C, and D are independent of x.

We can now compute

$$\overline{u'^2} = \frac{1}{L}\int_{x_0}^{x_0+L} u'^2\,dx = \frac{1}{L}\left(\int_{x_0}^{x_0+L_u} u'^2\,dx + \int_{x_1}^{x_1+L_d} u'^2\,dx\right) = \frac{1}{L}\left(\int_{x_0}^{x_0+L_u}\left[A + \left(\frac{x-x_0}{L}\right)B\right]^2 dx + \int_{x_1}^{x_1+L_d}\left[C + \left(\frac{x-x_1}{L}\right)D\right]^2 dx\right) = \frac{1}{L}\left[\left(A^2L_u + \frac{ABL_u^2}{2L} + \frac{B^2L_u^3}{3L^2}\right) + \left(C^2L_d + \frac{CDL_d^2}{2L} + \frac{D^2L_d^3}{3L^2}\right)\right]. \tag{A3}$$

Substituting and expanding, we find that

$$L\overline{u'^2} = \left\{\frac{L_d}{L}\left(\frac{L_u}{2}\right)\alpha + \left[\beta_0\left(\frac{1}{2}\right) - \beta_1\left(\frac{L_u - L_d}{2L}\right)\right]\right\}^2 L_u + \left\{\frac{L_d}{L}\left(\frac{L_u}{2}\right)\alpha + \left[\beta_0\left(\frac{1}{2}\right) = -\beta_1\left(\frac{L_u - L_d}{2L}\right)\right]\right\} \times [-L_d\alpha + (\beta_1 - \beta_0)]\frac{L_u^2}{2L} + [-L_d\alpha + (\beta_1 - \beta_0)]^2\frac{L_u^3}{3L^2} + \left\{-\left(\frac{L_u}{L}\right)\left(\frac{L_d}{2}\right)\alpha + \left[\left(\frac{1}{2} - \frac{L_u}{L}\right)\beta_0 - \frac{1}{2}\beta_1\right]\right\}^2 L_d + \left\{-\left(\frac{L_u}{L}\right)\left(\frac{L_d}{2}\right)\alpha + \left[\left(\frac{1}{2} - \frac{L_u}{L}\right)\beta_0 - \frac{1}{2}\beta_1\right]\right\}[L_u\alpha + (\beta_1 - \beta_0)]\frac{L_d^2}{2L} + [L_u\alpha + (\beta_1 - \beta_0)]^2\frac{L_d^3}{3L^2}, \tag{A4}$$

where

$$\alpha \equiv \frac{1}{\rho_0}\frac{\partial}{\partial z}[\rho_0(w_u - w_d)], \tag{A5}$$

$$\beta_0 \equiv (w_u - w_d)\frac{\partial x_0}{\partial z}, \tag{A6}$$

$$\beta_1 \equiv (w_u - w_d)\frac{\partial x_1}{\partial z}. \tag{A7}$$

We now separate out the three components given by Eqs. (A5)–(A7). We can write the α contribution as

$$\overline{u'^2} = (\alpha L)^2\frac{L_u^2L_d^2}{3L^4} = \frac{1}{3}\left[\frac{\sigma(1-\sigma)L}{\rho_0}\frac{\partial}{\partial z}[\rho_0(w_u - w_d)]\right]^2 \text{(alpha only)}. \tag{A8}$$

We can write the $\alpha\beta$ component as

$$L\overline{u'^2} = 2\frac{L_d}{L}\frac{L_u}{2}\alpha\left[\beta_0\left(\frac{1}{2}\right) - \beta_1\left(\frac{L_u - L_d}{2L}\right)\right]L_u + \frac{L_d}{L}\frac{L_u}{2}\alpha(\beta_1 - \beta_0)\frac{L_u^2}{2L} - \left[\beta_0\left(\frac{1}{2}\right) - \beta_1\left(\frac{L_u - L_d}{2L}\right)\right]L_d\alpha\frac{L_u^2}{2L} - 2L_d\alpha(\beta_1 - \beta_0)\frac{L_u^3}{3L^2} - 2\frac{L_u}{L}\frac{L_d}{2}\alpha\left[\left(\frac{1}{2} - \frac{L_u}{L}\right)\beta_0 - \frac{1}{2}\beta_1\right]L_d - \left(\frac{L_u}{L}\frac{L_d}{2}\right)\alpha(\beta_1 - \beta_0)\frac{L_d^2}{2L} + \left[\left(\frac{1}{2} - \frac{L_u}{L}\right)\beta_0 - \frac{1}{2}\beta_1\right]L_u\alpha\frac{L_d^2}{2L} + 2L_u\alpha(\beta_1 - \beta_0)\frac{L_d^3}{3L^2} = \frac{L_d}{L}L_u\alpha\left[\beta_0\left(\frac{1}{2}\right) - \beta_1\left(\frac{L_u - L_d}{2L}\right)\right]L_u + \frac{L_d}{L}\frac{L_u}{2}\alpha(\beta_1 - \beta_0)\frac{L_u^2}{2L} - \left[\beta_0\left(\frac{1}{2}\right) - \beta_1\left(\frac{L_u - L_d}{2L}\right)\right]L_d\alpha\frac{L_u^2}{2L} - 2L_d\alpha(\beta_1 - \beta_0)\frac{L_u^3}{3L^2} - \frac{L_u}{L}L_d\alpha\left[\left(\frac{1}{2} - \frac{L_u}{L}\right)\beta_0 - \frac{1}{2}\beta_1\right]L_d - \left(\frac{L_u}{L}\frac{L_d}{2}\right)\alpha(\beta_1 - \beta_0)\frac{L_d^2}{2L} + \left[\left(\frac{1}{2} - \frac{L_u}{L}\right)\beta_0 - \frac{1}{2}\beta_1\right]L_u\alpha\frac{L_d^2}{2L} + 2L_u\alpha(\beta_1 - \beta_0)\frac{L_d^3}{3L^2}. \tag{A9}$$

Simplifying further, we get

$$\overline{u'^2} = \frac{2L_uL_d}{3L^3}\alpha[(L_u^2 - L_d^2)(\beta_0 - \beta_1) + 2L_uL_d(\beta_0 + \beta_1)] \text{ (alpha-beta only).} \quad \text{(A10)}$$

Using Eqs. (A5)–(A7), (A10) can be written as

$$\overline{u'^2} = \frac{L\sigma(1-\sigma)}{3\rho_0}\frac{\partial}{\partial z}[\rho_0(w_u - w_d)^2]\left[(1-2\sigma) \times \left(\frac{\partial x_1}{\partial z} - \frac{\partial x_0}{\partial z}\right) + 2\sigma(1-\sigma)\left(\frac{\partial x_1}{\partial z} + \frac{\partial x_0}{\partial z}\right)\right]. \quad \text{(A11)}$$

The β contribution can be written as

$$\begin{aligned}
L\overline{u'^2} &= \left[\beta_0\left(\frac{1}{2}\right) - \beta_1\left(\frac{L_u - L_d}{2L}\right)\right]^2 L_u + \left[\beta_0\left(\frac{1}{2}\right) - \beta_1\left(\frac{L_u - L_d}{2L}\right)\right](\beta_1 - \beta_0)\frac{L_u^2}{2L} + (\beta_1 - \beta_0)^2\frac{L_u^3}{3L^2} \\
&\quad + (\beta_1 - \beta_0)^2\frac{L_d^3}{3L^2} + \left[\left(\frac{1}{2} - \frac{L_u}{L}\right)\beta_0 - \frac{1}{2}\beta_1\right]^2 L_d + \left[\left(\frac{1}{2} - \frac{L_u}{L}\right)\beta_0 - \frac{1}{2}\beta_1\right](\beta_1 - \beta_0)\frac{L_d^2}{2L} \\
&= \left[\beta_0\left(\frac{1}{2}\right) - \beta_1\left(\frac{L_u - L_d}{2L}\right)\right]\left\{\left[\beta_0\left(\frac{1}{2}\right) - \beta_1\left(\frac{L_u - L_d}{2L}\right)\right]L_u + (\beta_1 - \beta_0)\frac{L_u^2}{2L}\right\} + (\beta_1 - \beta_0)^2\left(\frac{L_u^3 + L_d^3}{3L^2}\right) \\
&\quad + \left[\left(\frac{1}{2} - \frac{L_u}{L}\right)\beta_0 - \frac{1}{2}\beta_1\right]\left\{\left[\left(\frac{1}{2} - \frac{L_u}{L}\right)\beta_0 - \frac{1}{2}\beta_1\right]L_d + (\beta_1 - \beta_0)\frac{L_d^2}{2L}\right\} \\
&= \left[\beta_0\left(\frac{1}{2}\right) - \beta_1\left(\frac{L_u - L_d}{2L}\right)\right]\left\{\beta_0\left(\frac{L_u}{2} - \frac{L_u^2}{2L}\right) + \beta_1\left[\frac{L_u^2}{2L} - \left(\frac{L_u - L_d}{2L}\right)L_u\right]\right\} + (\beta_1 - \beta_0)^2\left(\frac{L_u^3 + L_d^3}{3L^2}\right) \\
&\quad + \left[\left(\frac{1}{2} - \frac{L_u}{L}\right)\beta_0 - \frac{1}{2}\beta_1\right]\left\{\beta_0\left[\left(\frac{1}{2} - \frac{L_u}{L}\right)L_d - \frac{L_d^2}{2L}\right] + \beta_1\left(\frac{L_d^2}{2L} - \frac{L_d}{2}\right)\right\}. \quad \text{(A12)}
\end{aligned}$$

This can be simplified to

$$\begin{aligned}
L\overline{u'^2} &= \frac{L_uL_d}{2L}(\beta_0 + \beta_1)\left[\beta_0\left(\frac{L_u + L_d}{2L} + \frac{L_u - L_d}{2L}\right) + \beta_1\left(\frac{L_d - L_u}{2L} + \frac{L_u + L_d}{2L}\right)\right] + (\beta_1 - \beta_0)^2\left(\frac{L_u^3 + L_d^3}{3L^2}\right) \\
&= \frac{L_uL_d}{2L^2}(\beta_0 + \beta_1)(\beta_0L_u + \beta_1L_d) + (\beta_1 - \beta_0)^2\left(\frac{L_u^3 + L_d^3}{3L^2}\right) \text{ (beta only).} \quad \text{(A13)}
\end{aligned}$$

Using (17), (A6), and (A7), we can write this as

$$\overline{u'^2} = \overline{w'^2}\left[\frac{1}{2}\left(\frac{\partial x_0}{\partial z} + \frac{\partial x_1}{\partial z}\right)\left[\sigma\frac{\partial x_0}{\partial z} + (1-\sigma)\frac{\partial x_1}{\partial z}\right] + \left[\frac{1 - 3\sigma + 3\sigma^2}{3\sigma(1-\sigma)}\right]\left(\frac{\partial x_1}{\partial z} - \frac{\partial x_0}{\partial z}\right)^2\right] \text{ (beta only).} \quad \text{(A14)}$$

In (A14), we have also used the mass-flux relation $\overline{w'^2} = \sigma(1-\sigma)(w_u - w_d)^2$.

The total expression for the variance of the u wind ($\overline{u'u'}$) is the summation of Eqs. (A8), (A10), and (A13). This can be written as

$$\overline{u'^2} = \frac{(\alpha L)^2}{3}[\sigma(1-\sigma)]^2 + \frac{2L}{3}\alpha\sigma(1-\sigma)[(1-2\sigma) \times (\beta_1 - \beta_0) + 2\sigma(1-\sigma)(\beta_1 + \beta_0)] + \frac{1}{2}\sigma(1-\sigma) \times (\beta_0 + \beta_1)[\sigma\beta_0 + (1-\sigma)\beta_1] + (\beta_1 - \beta_0)^2\left(\frac{1 - 3\sigma + 3\sigma^2}{3}\right). \quad \text{(A15)}$$

We can compute this with LES if we can determine the value of β_0 and β_1 (or alternatively, $\partial x_0/\partial z$ and $\partial x_1/\partial z$). This is done in the main body of the paper.

b. $\overline{w'u'}$

$$\rho_0\overline{w'u'} = \frac{\rho_0}{L}\left(\int_{x_0}^{x_0+L_u} w_u u'\,dx + \int_{x_1}^{x_1+L_d} w_d u'\,dx\right) = \frac{\rho_0 w_u}{L}\left\{\int_{x_0}^{x_0+L_u}\left[A + \left(\frac{x-x_0}{L}\right)B\right]dx\right\}$$
$$+ \frac{\rho_0 w_d}{L}\left\{\int_{x_1}^{x_1+L_d}\left[C + \left(\frac{x-x_1}{L}\right)D\right]dx\right\} = \frac{\rho_0 w_u}{L}\left\{\frac{L_d}{L}\left(\frac{L_u}{2}\right)\frac{1}{\rho_0}\frac{\partial}{\partial z}\left[\rho_0\left(w_u - w_d\right)\right]\right.$$
$$\left. + \left(w_u - w_d\right)\left[\left(\frac{\partial x_0}{\partial z}\right)\left(\frac{1}{2}\right) - \left(\frac{\partial x_1}{\partial z}\right)\left(\frac{L_u - L_d}{2L}\right)\right]\right\}L_u + \frac{\rho_0 w_u}{L}\frac{L_u^2}{2L}\left\{-L_d\frac{1}{\rho_0}\frac{\partial}{\partial z}\left[\rho_0\left(w_u - w_d\right)\right]\right.$$
$$\left. + \left(w_u - w_d\right)\left(\frac{\partial x_1}{\partial z} - \frac{\partial x_0}{\partial z}\right)\right\} + \frac{\rho_0 w_d}{L}\left\{-\left(\frac{L_u}{L}\right)\left(\frac{L_d}{2}\right)\frac{1}{\rho_0}\frac{\partial}{\partial z}\left[\rho_0\left(w_u - w_d\right)\right] + \left(w_u - w_d\right)\right.$$
$$\left.\times\left[\left(\frac{1}{2} - \frac{L_u}{L}\right)\left(\frac{\partial x_0}{\partial z}\right) - \frac{1}{2}\left(\frac{\partial x_1}{\partial z}\right)\right]\right\}L_d + \frac{\rho_0 w_d}{L}\frac{L_d^2}{2L}\left\{L_u\frac{1}{\rho_0}\frac{\partial}{\partial z}\left[\rho_0\left(w_u - w_d\right)\right]\right.$$
$$\left. + \left(w_u - w_d\right)\left(\frac{\partial x_1}{\partial z} - \frac{\partial x_0}{\partial z}\right)\right\}. \tag{A16}$$

This simplifies considerably

$$\rho_0\overline{w'u'} = \left\{\frac{\rho_0 w_u}{L}\frac{1}{\rho_0}\frac{\partial}{\partial z}[\rho_0(w_u - w_d)]\right\}\left[\frac{L_d}{L}\left(\frac{L_u}{2}\right)L_u - \frac{L_u^2}{2L}L_d\right] + \left\{\frac{\rho_0 w_d}{L}\frac{1}{\rho_0}\frac{\partial}{\partial z}[\rho_0(w_u - w_d)]\right\}\left[-\left(\frac{L_u}{L}\right)\left(\frac{L_d}{2}\right)L_d\right.$$
$$\left. + \frac{L_d^2}{2L}L_u\right] + \frac{\rho_0}{L}(w_u - w_d)w_u\left\{\left[\left(\frac{\partial x_0}{\partial z}\right)\left(\frac{1}{2}\right) - \left(\frac{\partial x_1}{\partial z}\right)\left(\frac{L_u - L_d}{2L}\right)\right]L_u + \frac{L_u^2}{2L}\left(\frac{\partial x_1}{\partial z} - \frac{\partial x_0}{\partial z}\right)\right\}$$
$$+ \frac{\rho_0}{L}(w_u - w_d)w_d\left\{\left[\left(\frac{1}{2} - \frac{L_u}{L}\right)\left(\frac{\partial x_0}{\partial z}\right) - \frac{1}{2}\left(\frac{\partial x_1}{\partial z}\right)\right]L_d + \frac{L_d^2}{2L}\left(\frac{\partial x_1}{\partial z} - \frac{\partial x_0}{\partial z}\right)\right\}$$
$$= \frac{\rho_0}{L}(w_u - w_d)w_u L_u\left\{\left(\frac{\partial x_0}{\partial z}\right)\left(\frac{1}{2} - \frac{L_u}{2L}\right) + \left(\frac{\partial x_1}{\partial z}\right)\left[-\left(\frac{L_u - L_d}{2L}\right) + \frac{L_u}{2L}\right]\right\}$$
$$+ \frac{\rho_0}{L}(w_u - w_d)w_d L_d\left\{\left(\frac{\partial x_0}{\partial z}\right)\left[\left(\frac{1}{2} - \frac{L_u}{L}\right) - \frac{L_d}{2L}\right] + \left(\frac{\partial x_1}{\partial z}\right)\left(-\frac{1}{2} + \frac{L_d}{2L}\right)\right\}$$
$$= \frac{\rho_0}{L}(w_u - w_d)w_u L_u\left[\left(\frac{\partial x_0}{\partial z}\right)\frac{L_d}{2L} + \left(\frac{\partial x_1}{\partial z}\right)\frac{L_d}{2L}\right] + \frac{\rho_0}{L}(w_u - w_d)w_d L_d\left\{\left(\frac{\partial x_0}{\partial z}\right)\left[\left(\frac{1}{2} - \frac{L_u}{L}\right) - \frac{L_d}{2L}\right]\right.$$
$$\left. + \left(\frac{\partial x_1}{\partial z}\right)\left(-\frac{L_u}{2L}\right)\right\} = \frac{\rho_0}{L}(w_u - w_d)w_u L_u\frac{L_d}{2L}\left[\left(\frac{\partial x_0}{\partial z}\right) + \left(\frac{\partial x_1}{\partial z}\right)\right]$$
$$- \frac{\rho_0}{L}(w_u - w_d)w_d L_d\frac{L_u}{2L}\left[\left(\frac{\partial x_0}{\partial z}\right) + \left(\frac{\partial x_1}{\partial z}\right)\right] = \rho_0(w_u - w_d)^2\left(\frac{L_u L_d}{2L^2}\right)\left[\left(\frac{\partial x_0}{\partial z}\right) + \left(\frac{\partial x_1}{\partial z}\right)\right]. \tag{A17}$$

REFERENCES

André, J. C., G. DeMoor, P. Lacarrère, G. Therry, and R. Du-Vachat, 1978: Modeling the 24-hour evolution of the mean and turbulent structures of the planetary boundary layer. *J. Atmos. Sci.,* **35,** 1861–1883.

Betts, A., 1976: Modeling subcloud layer structure and interaction with a shallow cumulus layer. *J. Atmos. Sci.,* **33,** 2363–2382.

Bougeault, P., and J. C. André, 1986: On the stability of the third-order turbulence closure for the modeling of the stratocumulus-topped boundary layer. *J. Atmos. Sci.,* **43,** 1574–1581.

Brown, A. R., 1999: Large-eddy simulation and parameterization

of the effects of shear on shallow-cumulus convection. *Bound.-Layer Meteor.,* **91,** 65–80.

de Roode, S. R., P. G. Duynkerke, and A. P. Siebesma, 2000: Analogies between mass-flux and Reynolds-averaged equations. *J. Atmos. Sci.,* **57,** 1585–1598.

Etling, D., and R. A. Brown, 1993: Roll vortices in the planetary boundary layer: A review. *Bound.-Layer Meteor.,* **65,** 215–248.

Glendening, J. W., 1996: Lineal eddy features under strong shear conditions. *J. Atmos. Sci.,* **53,** 3430–3449.

Hicks, B. B., 1978: An analysis of Wangara micrometeorology: Surface stress, sensible heat, evaporation, and dewfall. NOAA Tech. Memo. ERL ARL-104, Air Resources Laboratories, Silver Spring, MD, 36 pp.

Khairoutdinov, M., and D. A. Randall, 2003: Cloud-resolving modeling of ARM summer 1997 IOP: Model formulation, results, uncertainties, and sensitivities. *J. Atmos. Sci.,* **60,** 607–625.

Lappen, C.-L., and D. A. Randall, 2001a: Toward a unified parameterization of the boundary layer and moist convection. Part I: A new type of mass flux model. *J. Atmos. Sci.,* **58,** 2021–2035.

——, and ——, 2001b: Toward a unified parameterization of the boundary layer and moist convection. Part II: Lateral mass exchanges and subplume-scale fluxes. *J. Atmos. Sci.,* **58,** 2036–2051.

——, and ——, 2001c: Toward a unified parameterization of the boundary layer and moist convection. Part III: Simulations of clear and cloudy convection. *J. Atmos. Sci.,* **58,** 2052–2072.

Moeng, C.-H., 1984: A large-eddy-simulation for the study of planetary boundary-layer turbulence. *J. Atmos. Sci.,* **41,** 2052–2062.

Randall, D. A., and G. J. Huffman, 1982: Entrainment and detrainment in a simple cumulus cloud model. *J. Atmos. Sci.,* **39,** 2793–2806.

——, Q. Shao, and C.-H. Moeng, 1992: A second-order bulk boundary-layer model. *J. Atmos. Sci.,* **49,** 1903–1923.

Schumann, U. and C.-H. Moeng, 1991: Plume fluxes in clear and cloudy convective boundary layers. *J. Atmos. Sci.,* **48,** 1746–1757.

Wang, S., and B. Albrecht, 1990: A mean-gradient model of the dry convective boundary layer. *J. Atmos. Sci.,* **47,** 126–138.

Willis, G. E., and J. W. Deardorff, 1974: Laboratory model of the unstable planetary boundary layer. *J. Atmos. Sci.,* **31,** 1297–1307.

Wu, X., and M. Yanai, 1994: Effects of vertical wind shear on the cumulus transport of momentum: Observations and parameterization. *J. Atmos. Sci.,* **51,** 1640–1660.